Distortion of the cholesteric planar texture in liquid crystals with a negative dielectric anisotropy

M. de Zwart

Classification
Physics Abstracts
61.30

DISTORTION OF THE CHOLESTERIC PLANAR TEXTURE IN LIQUID CRYSTALS WITH A NEGATIVE DIELECTRIC ANISOTROPY

M. DE ZWART

Philips Research Laboratories, Eindhoven, The Netherlands

(*Reçu le 28 septembre 1977, révisé le 16 décembre 1977, accepté le 22 décembre 1977*)

Résumé. — On étudie la formation de nouvelles régions planaires pendant la distorsion électrohydrodynamique de la texture planaire cholestérique de cristaux liquides à anisotropie diélectrique négative. En augmentant la tension, de nouvelles régions planaires apparaissent associées à un nombre croissant d'hélices dans la couche à conditions planaires limites constantes. La contraction du pas d'hélice qui en résulte s'effectue par des discontinuités reliées à des disclinations $S = (1)$. La stabilité des nouvelles régions planaires est favorisée par une importante anisotropie diélectrique négative. La tension limite pour la formation des réseaux quadratiques dans ces textures est sensiblement supérieure à celle théoriquement prévue par Helfrich et Hurault dont la théorie ne convient que pour des couches planaires cholestériques avec le pas d'hélice naturel p_0.

Abstract. — A study is made of the formation of new planar regions during the electrohydrodynamic distortion of the cholesteric planar texture in liquid crystals with a negative dielectric anisotropy. With increasing voltage successive planar regions are observed which are associated with an increasing number of helices across the layer with steady planar boundary conditions. The resulting pitch contraction occurs via discontinuities which can be related to $S = (1)$ disclinations. The stability of the new planar regions if favoured by a large negative dielectric anisotropy. The threshold voltage for the square grid perturbation of these induced textures is much larger than that predicted theoretically by Helfrich and Hurault, whose theory only holds for cholesteric planar layers in which the natural pitch p_0 occurs.

1. **Introduction.** — It has been known for many years that the planar texture of a cholesteric liquid crystal (the helical axis perpendicular to the substrates of the sample cell) can be disturbed by electric and magnetic fields. Upon application of an electric field parallel to the helical axis a deformation nucleates at a threshold voltage V_{th}. This deformation can be observed under a polarizing microscope as a square grid perturbation [1]. In the case of a cholesteric liquid crystal with a positive dielectric anisotropy

$$\Delta\varepsilon = \varepsilon_{\parallel} - \varepsilon_{\perp} > 0\,,$$

$\varepsilon_{\parallel}$ and $\varepsilon_{\perp}$ being the dielectric permittivity parallel and perpendicular, respectively, to the director a further increase of the field changes the orientation of the helical axis to a direction perpendicular to the applied field [2] and subsequently unwinds the helix inducing the nematic phase [3, 4]. When $\Delta\varepsilon < 0$ at low frequencies below the space-charge relaxation frequency, the square grid pattern is caused by electrohydrodynamic instabilities [5, 6]. In the case of a relatively small negative dielectric anisotropy

$$(\text{say } -1 \lesssim \Delta\varepsilon < 0)$$

a further increase of the electric field induces pronounced turbulence in the cholesteric texture (dynamic scattering). If the voltage is then switched off, the liquid crystal remains in a light-scattering disturbed texture, often called the *fingerprint* texture, in which the helical axis is, on average, aligned parallel to the electrodes [7, 8]. The transparent planar texture can be restored by applying a high-frequency voltage (above the space-charge relaxation frequency). This electro-optical effect can be used as a storage mode in liquid crystal displays [7].

In contrast to the effects described above, we found [9] in a liquid crystal with a relatively large negative dielectric anisotropy (α-cyanostilbene mixtures with $\Delta\varepsilon = -5$) that when the voltage is increased the square grid perturbation (Fig. 1*a*) is not followed by turbulence. On the contrary, a transformation is observed to a new planar texture (Fig. 1*b*, *c*) in which the original number of helices (n) across the layer has increased by one (a helix is defined as the 2π rotation of the director). In figure 2 this is shown schematically as A → B. We observe that this new planar texture B is nucleated at random positions in the perturbed texture A. Subsequently, texture B gradually dislodges

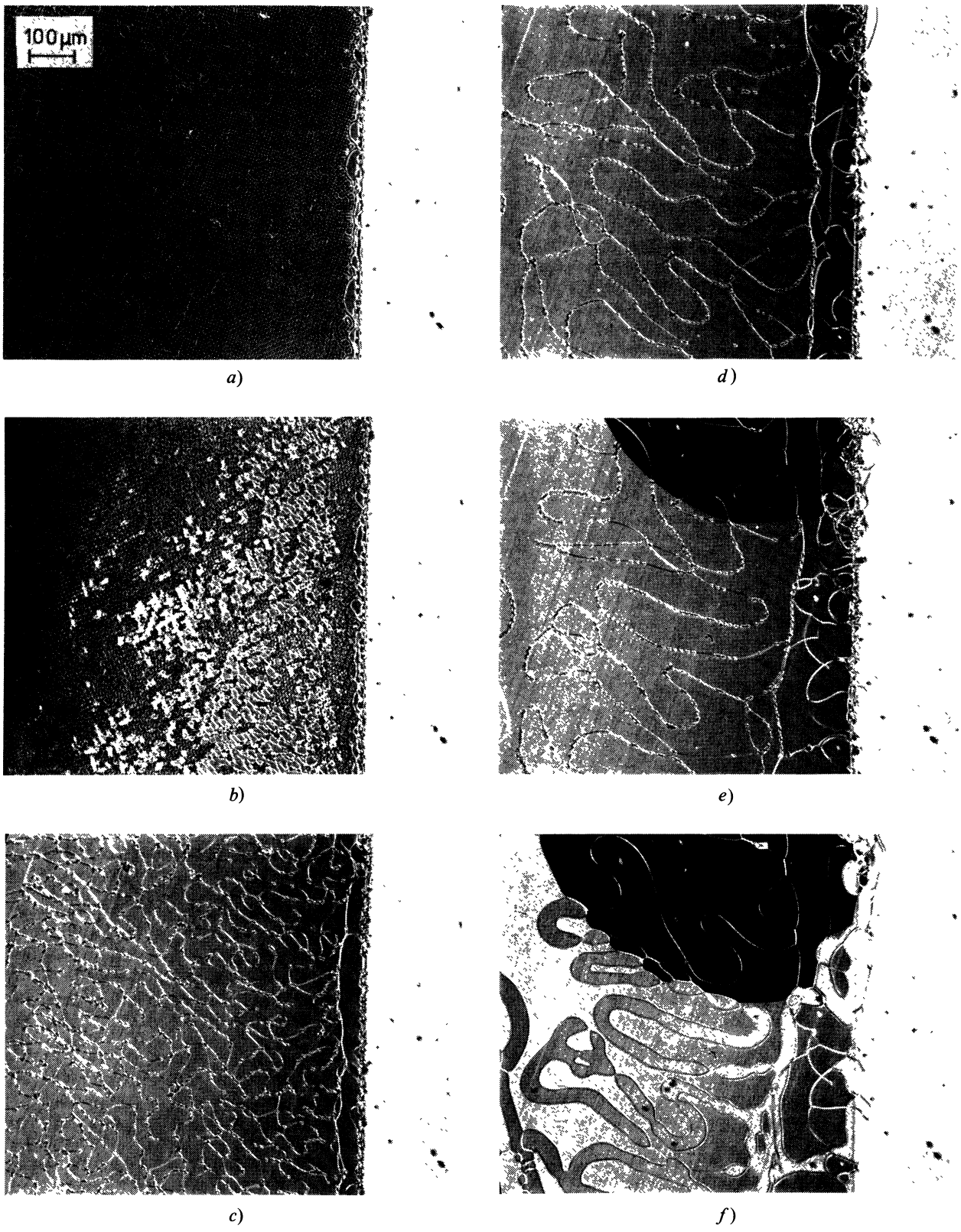

FIG. 1. — The electrohydrodynamic distortions and texture transformations in a cholesteric planar layer. The photographs show an area which is partly situated between the electrodes of a sample cell. *a*) $V = 10.5$ V ; *b*) $V = 10.8$ V ; *c*) $V = 11$ V ; *d*) $V = 11.5$ V ; *e*) $V = 12$ V ; *f*) $V = 0$.

the square grid perturbation of texture A, which is finally maintained in some thin disclination threads (Fig. 1*d*). As shown in ref. [9], a new square grid perturbation can be induced in texture B by raising the voltage further, the threshold voltage now being much higher (V_{th}(B) = 17.0 V).

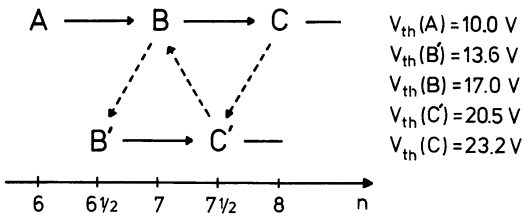

FIG. 2. — Scheme for the transformations of the original and induced planar regions (denoted by capitals) in the cholesteric mixtures. Solid arrows : transformations via the square grid perturbations in an increasing electric field. Dashed arrows : transformations via an $S = (\frac{1}{2})$ disclination line. V_{th} is the threshold voltage for the square grid perturbations in the corresponding planar region. The number of helices across the sample layer ($d/p = n$) in the various planar regions is indicated on the horizontal scale ; $d = 20$ μm.

On the other hand, if the voltage is increased very slowly or kept constant just after the formation of the new planar texture B($V \approx 11.5$ V), a third planar region can be nucleated spontaneously near imperfections in the cholesteric planar texture (B⋯→B'). This region, in which n has decreased by half a helix, slowly dislodges the previously induced planar texture B via a disclination line of strength $(\frac{1}{2})$ (Fig. 1*e*). Square grid perturbations in B' are formed at approximately the mean value of the threshold voltages for square grid perturbation in A and B. Thus, the formation of the planar region B' occurs only when the voltage of the applied electric field is between the square grid threshold of the A and B' textures.

At higher voltages this anomalous effect is observed several times in succession (B → C → etc.), but usually the planar textures become increasingly less stable. Finally electrohydrodynamical turbulence is observed. Figure 2 shows the complete transformation scheme. The solid arrows indicate the transitions via square grid perturbations. The dashed arrows give the transitions via an $S = (\frac{1}{2})$ disclination line. After the electric field is switched off the original texture A is formed everywhere by dislodging of the induced planar textures (Fig. 1*f*). This dislodging process occurs preferentially via $S = (1)$ disclinations

$$(C \Longrightarrow B \Longrightarrow A ; \quad C' \Longrightarrow B') .$$

Only the relaxation from texture B' to texture A takes place via an $S = (\frac{1}{2})$ disclination.

This paper describes an investigation of the mechanisms that lead to the occurrence and the stability of the induced planar textures. The experimental conditions are reported in section 2. The transitions to the induced planar regions are discussed in section 3. In section 4 the influence of the magnitude of the negative dielectric anisotropy on the occurrence and stability of the new planar textures is examined. Section 5 gives results for the measured threshold voltages in the various induced planar textures as a function of the frequency of the applied electric field and compares then with the predictions of the theory of Helfrich and Hurault in the low-frequency regime. The conclusions are presented in section 6.

2. **Experimental.** — The liquid crystal used in the experiments was a mixture of 68 % (by weight) of *p*-butoxy-*p'*-heptyl-α-cyano-*trans*-stilbene and 32 % *p*-ethoxy-*p'*-hexyloxy-α-cyano-*trans*-stilbene. This mixture is nematic between 15 °C and 58 °C. The static dielectric anisotropy is − 5.0 at 25 °C. The elastic constants for the twist and bend modes are respectively : $K_{22} = 5.2 \times 10^{-7}$ dyne and $K_{33} = 9.6 \times 10^{-7}$ dyne at 25 °C, as derived from the appropriate thresholds of the Fréderiks transitions in a magnetic field [10, 11].

The dielectric anisotropy of the α-cyanostilbene mixture is varied by additional mixing with the commercially available mixture ROTN-100 from Hoffmann-La Roche, which possesses a high positive dielectric anisotropy ($\Delta\varepsilon = + 25.0$ at 25 °C). The relation between the concentration of ROTN-100 and $\Delta\varepsilon$ is given in figure 3.

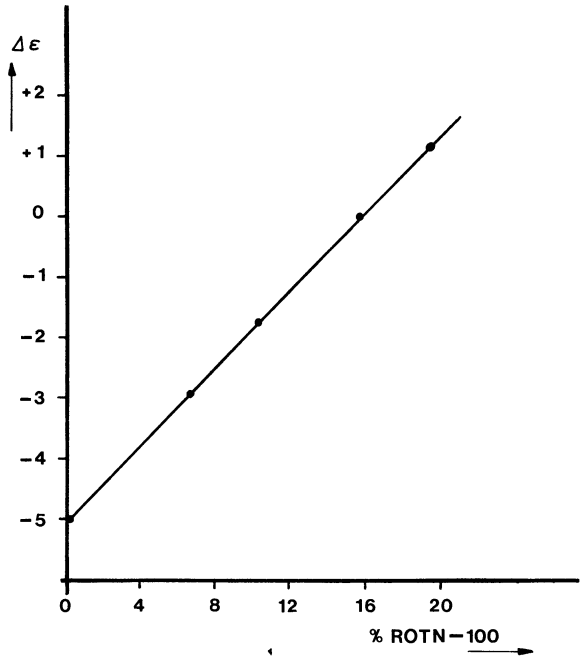

FIG. 3. — The static dielectric anisotropy $\Delta\varepsilon$ in the α-cyano-stilbene mixture versus the concentration (% by weight) of ROTN-100 at 25 °C.

A cholesteric phase is obtained by dissolving cholesteryl nonanoate (CN) in the nematic liquid crystal mixture. The natural pitch p_0 induced by this cholesteric material is determined in a Cano wedge, consisting of a cylindrical lens and a flat glass plate [12]. The amount of cholesteryl nonanoate added is 2.3 % by weight, resulting in a pitch p_0 of 3.3 ± 0.2 μm at 25 °C.

The sample cells consist of two parallel glass plates coated with transparent In_2O_3 electrodes and sepa-

rated by spacers. The thickness d of the liquid crystal layer is taken equal to the spacing of the empty cell, which is measured interferometrically with an accuracy of 0.5 %. By rubbing the electrodes unidirectionally prior to assembling the cell a uniform planar layer is obtained. The boundary conditions then constrain the number of helices across the layer to an integer or half-integer value. The actual pitch p, which will then in general be different from the natural value p_0, is determined by measuring the optical rotation of linearly polarized monochromatic light traversing the cholesteric planar layer parallel to the helical axis [13].

A polarizing microscope is used to observe the induced transitions in the texture of the cholesteric layer. Unless otherwise indicated, the measurements were performed at a frequency of 50 Hz and a temperature of 25 °C.

3. **The increase of the number of helices (n) across the layer in the induced planar textures.** — The number of helices in the electric field-induced planar textures obtained via the square grid perturbations always increases by one. An increase of half a helix was never observed, although this would also be compatible with the uniform planar boundary conditions. Transformations with a variation of half a helix only occur via the dislodging process of the initially induced planar texture with an $S = (\frac{1}{2})$ disclination line.

In order to account for this peculiar difference we consider the Volterra process whereby disclinations can be generated in an ordered medium [14]. Using this process Friedel and Kléman described the $S = (\frac{1}{2})$ and $S = (1)$ disclination lines in the cholesteric planar texture [15]. The $S = (\frac{1}{2})$ and $S = (1)$ lines are each dissociated into two independent line defects, called λ and τ defects. The possible combinations are shown in figure 4. Two $S = (\frac{1}{2})$ lines (Fig. 4*a*, *b*) and two $S = (1)$ lines (Fig. 4*c*, *d*) can be formed. In the cholesteric planar texture these discontinuities of a half and a whole helix are observed as single and double lines, respectively (Fig. 5, 7). An important difference between the λ and τ defects is the existence of a discontinuous change of the director at the core of the τ defect, while the λ defect has none. Thus, of the four possible combinations only the $\lambda^- \lambda^+$ defect pair possesses no singularity. This means that the $\lambda^- \lambda^+$ pair is energetically much more favourable than the other combinations. This is in agreement with the observation that in relatively thick cholesteric layers ($d \gtrsim 100$ μm) discontinuities of a whole helix occur much more frequently than discontinuities of half a helix [16].

The increase of n in the newly induced planar regions by a whole helix instead of half a helix can now be understood. Close observation of the disclinations in figure 4 shows that between the two line defects in a disclination the helical axis of the cholesteric texture is rotated by 90°. A helical turn without singular

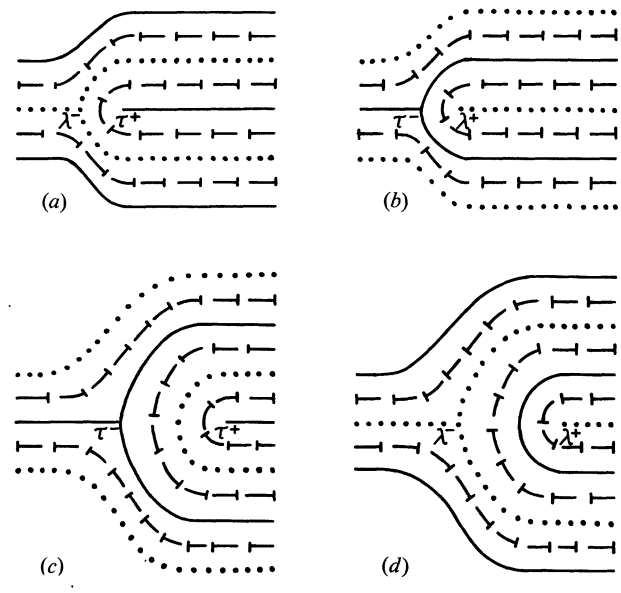

FIG. 4. — Combinations of line defects in single $S = (\frac{1}{2})$ (*a*, *b*) and double $S = (1)$, (*c*, *d*) Grandjean-Cano disclinations according to Volterra, ref. [15].

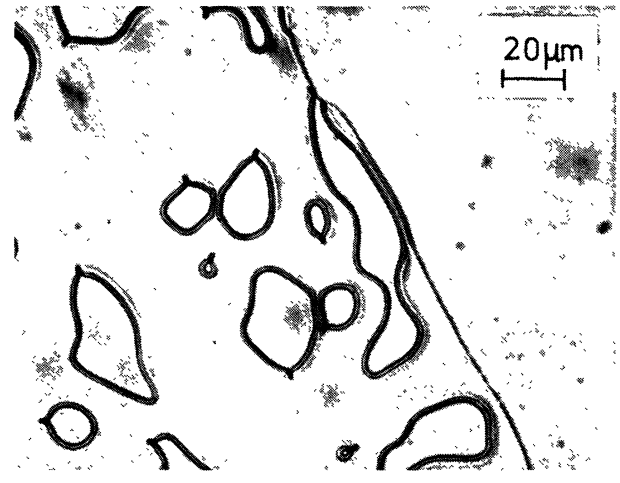

FIG. 5. — Double disclinations of strength $S = (1)$ surrounding newly induced planar regions in which the number of helices n across the layer has increased by one ; $V = 0$.

cores exists between the λ^- and λ^+ defects of the $\lambda^- \lambda^+$ pair (Fig. 4*d*). We assume that the formation of the new planar texture via the electrohydrodynamic distortion, whereby the helical axis is more or less tilted, occurs via these disclinations. The change to the new planar texture with an increase of a whole helix can then occur via the singularity-free $\lambda^- \lambda^+$ disclination. This transition is much more favourable than the other case of an increase with half a helix in spite of the fact that the latter texture has a lower energy density.

In contrast with the double lines the single lines are only formed in regions which are disturbed markedly by inhomogeneous electric fields, e.g. electrode edges and dust particles. Once nucleated, they diffuse into the previously induced planar regions and

there generate the new planar textures in which n is half a helix smaller, owing to the lower free energy density compared with the free energy of the previously induced planar texture.

In contrast to the $\lambda^- \lambda^+$ pair the $\tau^- \tau^+$ pair should hardly ever occur because it possesses two core singularities. This can be proved experimentally by considering closed double disclination lines. These lines are formed when the electric field is switched off immediately after the nucleation of the new planar regions in the square grid pattern, for instance, just after the formation of texture B in the perturbed texture A (Fig. 1*b*, *c*). The closed disclinations surround regions in which n has increased by one (Fig. 5). A remarkable phenomenon is the presence of small discontinuities or *tails* in all the closed lines. These *tails* result from the absence of the $\tau^- \tau^+$ or $\lambda^- \lambda^+$ pair from these closed lines. The geometry of a closed double disclination line is given in figure 6. This disclination line, described by Bouligand [17], is constructed in such a way that only the $\lambda^- \lambda^+$ occurs. Because of the absence of the $\tau^- \tau^+$ pair, there must be at least one position in the closed line where the cholesteric planes in which the disclinations are located are shifted half a helix along the helical axis.

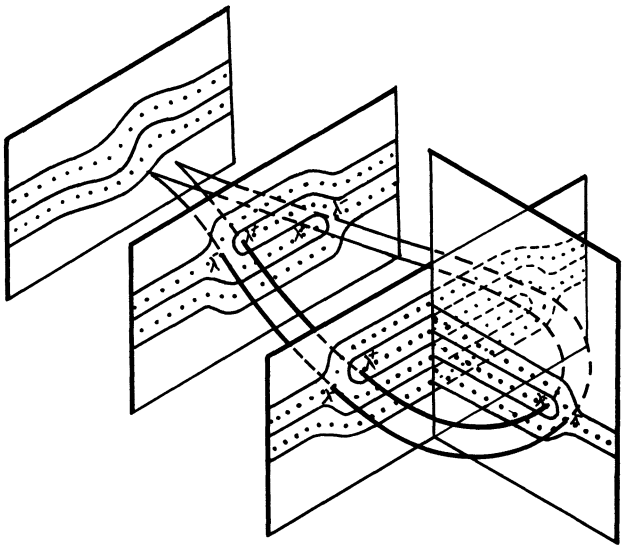

FIG. 6. — Closed double disclination line consisting of a $\lambda^- \lambda^+$ defect pair, ref. [17].

At this position a discontinuity is created that corresponds to the observed small *tail*. The same configuration should also occur with only the $\tau^- \tau^+$ pair in the loop. On the other hand a closed single line surrounding an area in which n has increased by half a helix is always found to be continuous ; it possesses no *tail* (Fig. 7). This means that the single line has to remain in the same cholesteric planes along the whole circle. In this case the two possible combinations of the $\lambda\tau$ pair ($\lambda^- \tau^+$ and $\tau^- \lambda^+$) must occur as such in the loop.

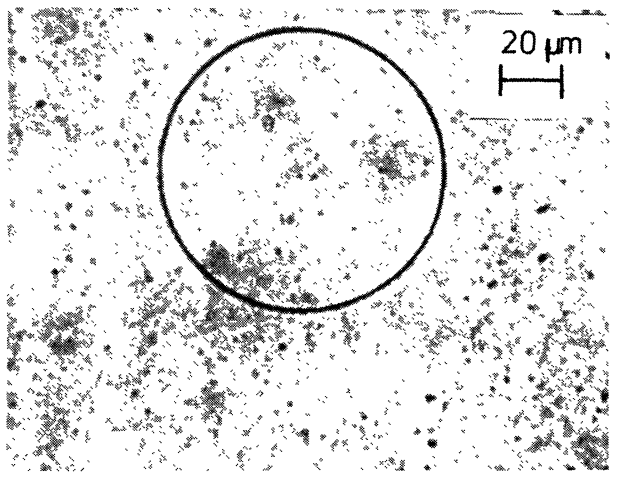

FIG. 7. — Single disclination of strength $S = (\frac{1}{2})$ surrounding a region in which n has increased by half a helix ; $V = 0$.

The occurrence of only one defect pair in the closed double lines, which is in contrast to the configuration of the closed single lines, agrees with the idea that an energy difference must exist between λ and τ defects. The $\lambda^- \lambda^+$ combination then apparently has the lowest core energy and is most probably the defect pair from which the double disclination lines are constituted.

4. **Variation of the dielectric anisotropy.** — As described above, the new planar regions occur after the electric field-induced perturbations in the cholesteric planar texture of the α-cyanostilbene/CN mixture. However, if this texture is distorted by an increasing magnetic field parallel to the helical axis only the usual square grid perturbation is observed, followed by focal conic texture and finally the unwinding of the helical structure. Furthermore, in the cholesteric planar texture of liquid crystals with a *positive* dielectric anisotropy we failed to observe the newly induced planar textures upon increasing magnetic as well as electric fields. The successive creation of square grid perturbations and induced planar textures in the liquid crystal with a *negative* dielectric anisotropy is obviously related to the presence of both the disturbing torque due to the induced space charges and the dielectric torque $\Gamma_{\text{diel.}} \propto |\Delta\varepsilon| E^2$, which stabilizes the cholesteric planar texture. We therefore examined the influence of the dielectric anisotropy, using the mixtures described in section 2. The anisotropy of the conductivity and the mean conductivity were kept practically constant. The successive formation of square grid patterns and planar regions in an increasing electric field can be recorded by using the measurements of the transmission of a He-Ne laser beam through the sample cells. Figure 8 shows the different transmittance curves for various $\Delta\varepsilon$ values versus the voltage, which was increased by 0.1 V/s. From curve a it can be clearly observed that after the occurrence of the first deformations (the dips correspond to the square grid perturbations) the layer returns

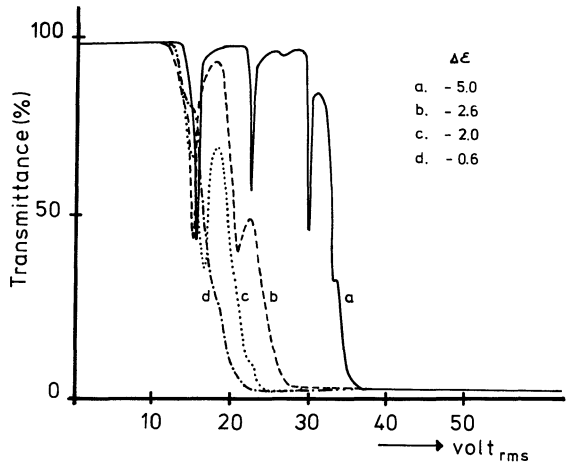

FIG. 8. — Transmittance as a function of an increasing voltage (0.1 V/s) in the α-cyanostilbene/ROTN-100/CN mixtures. The amount of ROTN-100 : *a*) 0 %; *b*) 7.5 %; *c*) 9.5 %; *d*) 13.9 % (by weight).

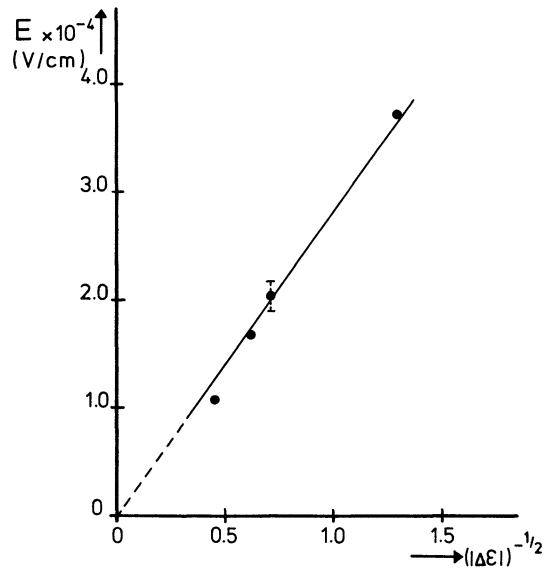

FIG. 9. — Erasing field (4 kHz) of the storage mode in the α-cyanostilbene/ROTN-100/CN mixtures versus the dielectric anisotropy. The erasure time is 1 s.

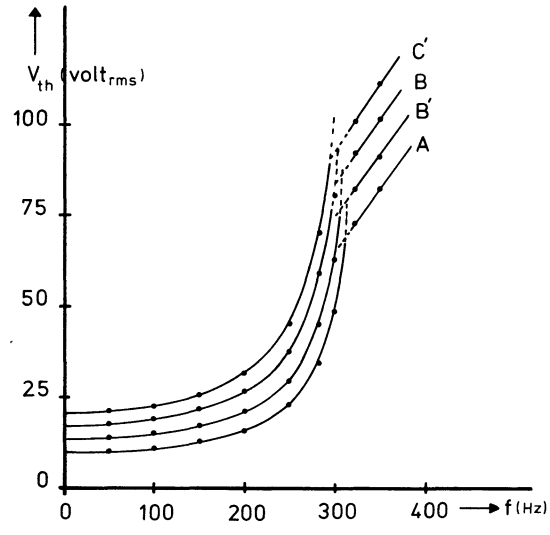

FIG. 10. — Threshold voltage V_{th} for the electrohydrodynamic distortions in the original and induced cholesteric planar textures of the α-cyanostilbene/CN mixture versus the frequency of the applied AC field. Sample thickness is 20 μm; the mean conductivity is $2 \times 10^{-9}\ \Omega^{-1}\ cm^{-1}$.

several times in succession to the transparent planar texture. Because the rate of increase of the voltage is relatively fast, only planar textures in which n changes sequentially by one occur. The transmittance curves for the mixtures with a smaller negative dielectric anisotropy (curves b and c) show a decrease in the number of the induced planar textures, which are also less stable. In the liquid crystal mixture with $\Delta\varepsilon = -0.6$ (curve d) no new planar textures are induced at all. The successive occurrence of square grid perturbations and planar regions causes a large negative dielectric anisotropy to have a suppressing effect on possible turbulence, which means that in these liquid crystals the optical storage mode induced by turbulence can only be obtained at relatively high voltages. On the other hand, the erasure of this storage mode can be performed via the dielectric torque. Hence, a large negative dielectric anisotropy enables us to erase the memory at lower voltages. This effect was investigated for the α-cyanostilbene/ROTN-100/CN mixtures. The voltages necessary for erasing in 1 s are plotted in figure 9. We see that an increase of the negative dielectric anisotropy decreases the erasure voltage of the storage mode but at the cost of increasing the writing voltage.

5. **The threshold voltage V_{th} in the successively induced planar textures.** — 5.1 PLANAR SAMPLE CELL. — We mentioned in Section 1 that each newly induced planar texture possesses a higher threshold voltage for new square grid perturbations. The increase is about 7 V for a planar texture in which the number of helices has increased by one. The threshold voltage V_{th} in the various planar textures as a function of the frequency of the applied AC field is given in figure 10. The new planar textures are formed in both the *conduction* regime and the *dielectric* regime. In both regimes the differences between the various thresholds are approximately constant.

Helfrich [18, 19] and Hurault [20] have made theoretical predictions for the static deformation of the cholesteric planar texture with a pitch p in the low-frequency fields. For the RMS value of the threshold voltage at which the square grid perturbations arise with the condition $n = d/p \gg 1$ Hurault derived :

$$V_{th}^2 = \frac{8\pi^3}{\varepsilon_\perp} \cdot \frac{\varepsilon_\perp + \varepsilon_\parallel}{\varepsilon_\perp - \varepsilon_\parallel} \cdot \frac{1 + \omega^2\tau^2}{\zeta - 1 - \omega^2\tau^2} \times \left(\frac{3}{2} K_{22} K_{33}\right)^{1/2} \frac{d}{p}, \quad (1)$$

where ω is the frequency of the excitation field and τ the space-charge relaxation time. The parameter ζ is given by :

$$\zeta = 1 - \frac{\sigma_{\parallel} - \sigma_{\perp}}{\sigma_{\parallel} + \sigma_{\perp}} \cdot \frac{\varepsilon_{\parallel} + \varepsilon_{\perp}}{\varepsilon_{\parallel} - \varepsilon_{\perp}}$$

where $\sigma_{\parallel}$ and $\sigma_{\perp}$ are the conductivities parallel and perpendicular, respectively, to the director. The wavelength Λ of the square grid perturbation at threshold is given by :

$$\Lambda^2 = \left(\frac{3}{2} \cdot \frac{K_{33}}{K_{22}}\right)^{1/2} pd . \qquad (2)$$

The square of the threshold voltages for square grid perturbation in the original and newly induced planar textures of the α-cyanostilbene/CN mixture is plotted as a function of n in figure 11 (circles). Using the Frank elastic constants K_{22} and K_{33}, found from the Fréderiks transition in the nematic state (section 2), the theoretical values of $V_{th}^2(\sigma_{\parallel}/\sigma_{\perp} = 1.25\,;\, \varepsilon_{\perp} = 11.0)$ can be calculated via eq. (1) with the condition $\omega^2 \tau^2 \ll 1$. These values are plotted as the solid line in figure 11. The threshold voltage in the original planar texture A in which the natural pitch p_0 exists agrees with these theoretical predictions. However, the threshold voltages in the newly induced planar textures deviate markedly from the theoretical curve. As we shall show, eq. (1) is valid for the natural pitch p_0 only.

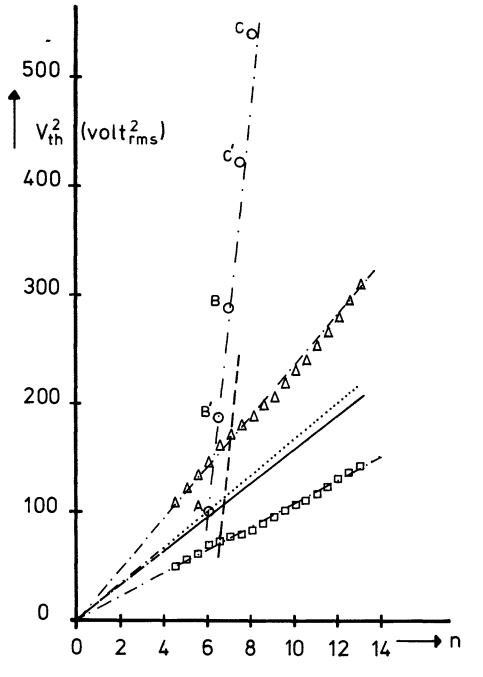

FIG. 11. — Dependence of the threshold voltage V_{th} at low frequencies on the number of helices n across the cholesteric planar layer of the α-cyanostilbene/CN mixture. The circles, obtained from a parallel sample cell, correspond to the original (labelled A) and induced (B' ... C) planar regions. The squares and triangles, obtained from a wedge-shaped cell, are the values on the wide and narrow side, respectively, of the strips between two successive Grandjean-Cano disclination lines. The dashed line connects a square and a triangle corresponding to both sides of the same disclination line (cell thickness the same, n differing by half a helix). The dotted line, halfway between the straight lines through the squares and triangles, represents the experimental data for $p = p_0$: the solid line gives the theoretical predictions of eq. (1).

5.2 WEDGE-SHAPED SAMPLE CELL. — In addition to the above results we performed measurements in a wedge-shaped sample cell (wedge angle = 15' ; d = 10-60 μm). Owing to the unidirectional rubbing of the electrodes many single equally spaced Grandjean-Cano disclination lines are observed in the cholesteric planar texture (Fig. 12). These lines are formed as a consequence of a discontinuity of a half in the number of helices across the layer [21, 22]. The pitch has the natural value p_0 in the middle of a strip between two successive disclination lines [23], but increases towards the wide side of the cell and decreases towards the narrow side.

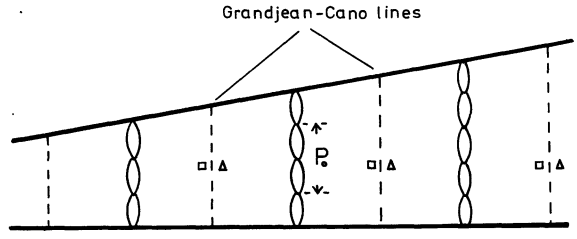

FIG. 12. — Unidirectionally rubbed wedge-shaped sample cell. The cholesteric planar layer possesses equally spaced single Grandjean-Cano lines. The squares and triangles denote the positions of the corresponding threshold voltages indicated in figure 11.

In such a cell Scheffer [24], Gerritsma and van Zanten [25] and Rault [26] found that the threshold for square grid perturbations induced by electric and magnetic fields depends on the contraction or stretching of the pitch induced by the boundary conditions. This effect cannot be accounted for by the Helfrich and Hurault theory according to which the threshold voltage depends only on the number of helices across the planar layer.

In analogy to these experiments we find that when the electric field across the wedge-shaped layer of the α-cyanostilbene/CN mixture is increased the square grid perturbations always appear first at the wide side of the strips and expand uniformly across them towards the narrow side. In figure 11 the square of the threshold voltage near the disclinations at the wide side (squares) and narrow side (triangles) of the strips is plotted as a function of n. From these curves we note that the square of the threshold voltages at the same positions in the different strips is proportional to the number of helices across the planar layer. The curves can be extrapolated to the origin, but the slopes differ considerably. The threshold voltage in the regions with the natural pitch is given by the

straight dotted line, which also passes through the origin on extrapolation. This curve for p_0 agrees very well with the values calculated via eq. (1).

In the same wedge-shaped cell we measured the wavelengths of the static square grid perturbations for p_0 in the middle of the strips. Figure 13 gives Λ^2 versus the number of helices n across the layer. Using eq. (2) with K_{22} and K_{33} we calculated the theoretical values of Λ^2 for the natural pitch p_0 (solid line).

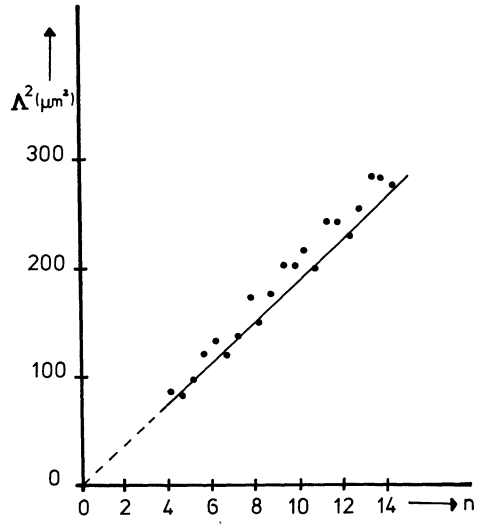

FIG. 13. — The square of the wavelength of the square grid perturbations at threshold versus the number of helices with the natural pitch p_0. These values were measured in a wedge-shaped cell filled with the α-cyanostilbene/CN mixture. The solid line gives the theoretical predictions of eq. (2).

In view of the experimental accuracy of ± 20 % for the measurements in the wedge-shaped cell there is good agreement between the experimental data and calculated values for textures with the natural pitch. On the other hand the threshold voltage in the wedge-shaped cell changes markedly towards the wide and narrow side of a strip. The dashed curve in figure 11 shows the variation of the threshold voltage between a contracted and stretched configuration of the pitch that is caused by a change of n by half a helix across a layer of constant thickness. This line connects V_{th}^2 on both sides of a single Grandjean-Cano disclination line in the wedge-shaped sample cell. The slope of this curve corresponds quite well with the slope of the curve which gives the increase of V_{th}^2 in the induced planar regions generated in the parallel sample cell (B' ... C).

To check whether the change of the negative dielectric anisotropy brings about a change of the threshold voltages for square grid perturbations, we measured the threshold voltages of the α-cyanostilbene/ROTN-100/CN mixtures with different $\Delta\varepsilon$ in the same wedge-shaped cell. We find that there is no appreciable difference from the threshold variation of the liquid crystal with $\Delta\varepsilon = -5$. (Note : with the condition $\omega^2 \tau^2 \ll 1$, eq. (1) reduces to

$$V_{th}^2 = (8\pi^3/\varepsilon_\perp).(\sigma_\parallel + \sigma_\perp)/(\sigma_\parallel - \sigma_\perp) \times \times (\tfrac{3}{2} K_{22} K_{33})^{1/2}.d/p).$$

6. **Conclusion.** — It is found that the formation of new planar textures during the electrohydrodynamic distortion of a cholesteric planar texture with steady boundary conditions has a considerable effect in counteracting the occurrence of turbulence. The formation and stability of the new planar textures depend largely on the magnitude of the negative dielectric anisotropy. A larger negative dielectric anisotropy with a correspondingly larger dielectric torque results in a higher stability so that the planar texture is more easily formed.

There is a large difference between the threshold voltages for the electrohydrodynamic deformation in these successively induced planar regions. This difference does not depend on the dielectric anisotropy, but is caused by a contraction of the pitch. This pitch contraction occurs as a consequence of the increase of the number of helices across the planar layer during the transition to the new planar texture. With increasing voltage the number of helices always increases by one, because this situation can occur without the nucleation of singularities in the cholesteric texture. The variation of the threshold voltages under these circumstances, which will be subjected to a further investigation, differs considerably from the theoretical predictions of Helfrich and Hurault. Their theory is valid only in cholesteric planar textures in which the pitch is equal to the natural pitch.

Acknowledgment. — The author wishes to thank Th. W. Lathouwers and J. L. A. M. Heldens for practical assistance and W. A. P. Claassen and F. Leenhouts for measuring the elastic constants.

References

[1] GERRITSMA, C. J. and VAN ZANTEN, P., *Phys. Lett.* **37A** (1971) 47.

[2] KAHN, F. J., *Phys. Rev. Lett.* **24** (1970) 209.

[3] WYSOCKI, J., ADAMS, J. and HAAS, W., *Phys. Rev. Lett.* **20** (1968) 1024.

[4] BAESSLER, H. and LABES, M. M., *Phys. Rev. Lett.* **21** (1968) 1971.

[5] RONDELEZ, F. and ARNOULD, H., *C. R. Hebd. Séan. Acad. Sci.* **273B** (1971) 549.

[6] RONDELEZ, F., ARNOULD, H. and GERRITSMA, C. J., *Phys. Rev. Lett.* **28** (1972) 735.

[7] HEILMEYER, G. H. and GOLDMACHER, S. E., *Appl. Phys. Lett.* **13** (1968) 132.

[8] HAAS, W., ADAMS, J. and FLANNERY, J. B., *Phys. Rev. Lett.* **24** (1970) 577.

[9] DE ZWART, M. and LATHOUWERS, Th. W., *Phys. Lett.* **55A** (1975) 41.

[10] DE JEU, W. H., CLAASSEN, W. A. P. and SPRUIJT, A. M. J., *Mol. Cryst. Liq. Cryst.* **37** (1976) 269.
[11] LEENHOUTS, F., VAN DER WOUDE, F. and DEKKER, A. J., *Phys. Lett.* **58A** (1976) 242.
[12] CANO, R. and CHATELAIN, P., *C. R. Hebd. Séan. Acad. Sci.* **253** (1961) 1815.
[13] DE VRIES, Hl., *Acta Crystallogr.* **4** (1951) 219.
[14] See for instance, FRIEDEL, J., *Dislocations* (Pergamon, London) 1964.
15. KLÉMAN, M. and FRIEDEL, J., *J. Physique Colloq.* **30** (1969) (C4) 43.
[16] Orsay Group, *Phys. Lett.* **28A** (1969) 687 ; *J. Physique Colloq.* **30** (1969) (C4) 38.
[17] BOULIGAND, Y., *J. Physique* **35** (1974) 959.
[18] HELFRICH, W., *Appl. Phys. Lett.* **17** (1970) 531.
[19] HELFRICH, W., *J. Chem. Phys.* **55** (1971) 839.
[20] HURAULT, J. P., *J. Chem. Phys.* **59** (1973) 2068.
[21] GRANDJEAN, F., *C. R. Hebd. Séan. Acad. Sci.* **172** (1921) 71.
[22] CANO, R., *Bull. Soc. Fr., Minéral. Cristallogr.* **90** (1967) 90, 333 ; **91** (1968) 20.
[23] GERRITSMA, C. J., GOOSSENS, W. J. A. and NIESSEN, A. K., *Phys. Lett.* **34A** (1971) 354.
[24] SCHEFFER, T. J., *Phys. Rev. Lett.* **28** (1972) 593.
[25] GERRITSMA, C. J. and VAN ZANTEN, P., *Liquid Crystals and Ordered Fluids* 2, Edited by J. F. Johnson and R. S. Porter (Plenum, New York) 1974, 437.
[26] RAULT, J., *Liquid Crystals and Ordered Fluids* 2, Edited by J. F. Johnson and R. S. Porter (Plenum, New York) 1974, 677.